

Dynamic control of quantum geometric heat flux in nonequilibrium spin-boson model

Tian Chen,¹ Xiang-Bin Wang,^{1,2,*} and Jie Ren^{3,†}

¹State Key Laboratory of Low Dimensional Quantum Physics, Department of Physics,
Tsinghua University, Beijing 100084, People's Republic of China

²Jinan Institute of Quantum Technology, Shandong Academy of Information
and Communication Technology, Jinan 250101, People's Republic of China

³Theoretical Division, Los Alamos National Laboratory, Los Alamos, New Mexico 87545, USA

We study the quantum geometric heat flux in the nonequilibrium spin-boson model. By adopting the noninteracting-blip approximation, we show that there exists the geometric heat flux only when the two level system is nondegenerate. Moreover, the pumping, no pumping, and dynamic control of geometric heat flux are discussed in detail, compared to the results with Redfield-weak coupling approximation. In particular, two system-bath couplings modulation induced geometric energy transfer is identified, which is exclusive to quantum transport in the strong system-bath coupling regime.

PACS numbers: 44.90.+c, 03.65.Vf, 05.60. Gg, 05.70. Ln

Introduction. Smart energy control in low dimensional nanoscale systems is of both theoretical and practical importance, rendering the emergence of Phononics [1]. As is well known, according to the second law of thermodynamics, energy cannot transfer from a cold reservoir to a hot side without external modulation. In order to obtain a more flexible control of thermal energy at nanoscale, there is a great demand in designing intriguing phononic devices, which can utilize temporal modulations to achieve dynamic control, such as in heat pump, motor and engine.

So far, many proposals have been provided to control the energy flow between a cold reservoir and a hot one [2–9]. As a result of these investigations [3, 6], there is no way to pump the energy from the cold side to the hot side in classical-oscillator systems by force driving, though heat pump can be implemented in classical spin chains [3]. An interesting design to realize the heat transfer is using the adiabatic modulation [10, 11]. In particular, Ref. [10] proposed to pump the energy between two reservoirs with equal temporal-averaged-temperature by utilizing the geometric phase induced heat transfer. Very recently, similar geometric heat flux in classical interacting systems is also studied [11].

There are many approximation methods in studying the heat transfer in spin-boson model [10, 12–17]. Among them, the Redfield-weak coupling approximation is often used since this method is effective. However, recent studies reveal that there are also limitations to the Redfield-weak coupling scheme [15–19]. Besides this scheme, other methods such as the multilayer multiconfiguration Hartree [15] and the noninteracting-blip approximation (NIBA) [20–22] are also applied to study the heat flow under temperature bias. Interestingly, these methods can produce results different from that of the Redfield approximation method for the same Hamiltonian. In particular, as shown in Refs. [15, 17], the heat current is not linearly dependent on the system-bath interaction strength as given by the Redfield-weak coupling scheme. The maximal

heat current exists at the intermediate system-reservoir coupling strength[15, 17], and then the heat current descends as increasing the system-reservoir coupling strength. So far, different physical results of Redfield scheme and NIBA are not found in the weak system-bath interaction regime.

There are mainly two assumptions inherent in the Redfield-weak coupling scheme. One is the *resonant tunneling* between the system and the reservoirs, and only the resonant frequency in the reservoir contributes to the dynamics. The other is that each individual reservoir interacts with the system *separately*, or say, *additively*. In this paper, we shall not use these two assumptions, but adopt the NIBA scheme to study the geometric phase induced energy transfer. The effect of non-resonant tunneling between the system and the reservoirs as well as their collective non-additive interacting are both considered. We shall first review the analytical expressions of the investigated spin-boson model in NIBA, and the geometric phase induced energy transfer through the generating function approach. We then investigate in detail the behaviors of geometric heat flux under various modulation protocols.

Our contributions are two-folds. First, we find different results of the two methods (Redfield and NIBA) with whatever system-bath interaction strength through calculating the geometric phase induced heat flux in unbiased (degenerate) case. This renders the geometric heat flux could become an effective tool to compare the difference or even judge the correctness of various approximation schemes. Second, geometric heat flux itself is a very important physical problem. A more thorough investigation to the problem with different methods is meaningful. We find that the temperatures-modulation-induced geometric heat flux are absent under the unbiased case, while linearly dependent on the system-bath coupling strength under the biased (nondegenerate) case. Also, additional to reversing the modulation protocol, the direction of geometric heat flux can be reversed by adjusting the system's parameters. Moreover, two system-bath couplings modulation induced geometric heat flux is identified. So far, this nontrivial observation is exclusive for quantum transport in the strong system-bath coupling regime.

Model. The non-equilibrium spin-boson (NESB) model, [see the left panel of Fig. 1], consisting of a two-level sys-

*Electronic address: xbwang@mail.tsinghua.edu.cn

†Electronic address: renjie@lanl.gov

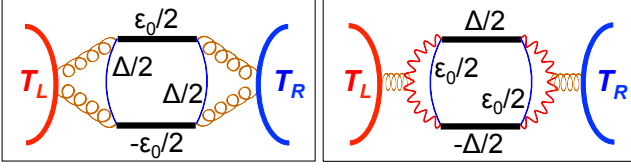


FIG. 1: (color online). Schematic illustrations of the nonequilibrium spin-boson model for energy transfer. The left panel describes the Hamiltonian (1) while the right one depicts the Hamiltonian (2). They are equivalent, with only a rotation difference of the basis.

tem in contact with two bosonic reservoirs with temperatures T_ν ($\nu = L, R$), is described by the Hamiltonian:

$$H = \frac{\varepsilon_0}{2}\sigma_z + \frac{\Delta}{2}\sigma_x + \sigma_z \sum_{\nu,j} \lambda_{j,\nu} (b_{j,\nu}^\dagger + b_{j,\nu}) + \sum_{\nu,j} \omega_{j,\nu} b_{j,\nu}^\dagger b_{j,\nu}, \quad (1)$$

where ε_0 is the energy gap of the two levels; Δ denotes the tunneling between them; $\sigma_z \equiv |1\rangle\langle 1| - |0\rangle\langle 0|$ and $\sigma_x \equiv |0\rangle\langle 1| + |1\rangle\langle 0|$ are the Pauli matrices expressed in the two level basis; $b_{j,\nu}^\dagger$ ($b_{j,\nu}$) denotes the creation (annihilation) operator of the j th harmonic mode in the ν bosonic bath, with $\lambda_{j,\nu}$ the system-bath coupling strength. We can also rotate the Hamiltonian (1) firstly around the y axis by an angle $\pi/2$, then around the new x axis by an angle π . In this way, $\sigma_x \rightarrow \sigma_z$, $\sigma_z \rightarrow \sigma_x$, and the alternative equivalent Hamiltonian reads, [see the right panel of Fig. 1]:

$$H = \frac{\varepsilon_0}{2}\sigma_x + \frac{\Delta}{2}\sigma_z + \sigma_x \sum_{\nu,j} \lambda_{j,\nu} (b_{j,\nu}^\dagger + b_{j,\nu}) + \sum_{\nu,j} \omega_{j,\nu} b_{j,\nu}^\dagger b_{j,\nu}. \quad (2)$$

Throughout the paper, we will work in the basis of Hamiltonian (1) in the NIBA scheme. Before proceeding to the energy transport, it is useful to transform the NESB Hamiltonian (1) by using the canonical transformation [23] (also called Lang-Firsov or polaron transformation): $H_T = U^\dagger H U$, $U = \exp[i\sigma_z \Omega/2]$, $\Omega = 2i \sum_{\nu,j} \frac{\lambda_{j,\nu}}{\omega_{j,\nu}} (b_{j,\nu}^\dagger - b_{j,\nu})$. After neglecting an irrelevant constant $-\sum_{j,\nu} \lambda_{j,\nu}^2/\omega_{j,\nu}$, the transformed Hamiltonian is expressed as:

$$H_T = \frac{\varepsilon_0}{2}\sigma_z + \frac{\Delta}{2}(\sigma_+ e^{-i\Omega} + \sigma_- e^{i\Omega}) + \sum_{j,\nu} \omega_{j,\nu} b_{j,\nu}^\dagger b_{j,\nu}, \quad (3)$$

with $\sigma_+ \equiv (\sigma_x + i\sigma_y)/2 = |1\rangle\langle 0|$ and $\sigma_- \equiv (\sigma_x - i\sigma_y)/2 = |0\rangle\langle 1|$. H_T clearly shows that the energy transfer is accomplished by the excitation from the lower level to the upper one with absorbing energy from the baths, and the relaxation from the upper level to the lower one with releasing energy to the baths. Thereafter, as a result of the NIBA method [19–22] and with the Markov assumption, the population dynamics of the two-level system becomes [17]:

$$\frac{d}{dt} \begin{pmatrix} p_0(t) \\ p_1(t) \end{pmatrix} = - \begin{pmatrix} K(-\varepsilon_0) & -K(\varepsilon_0) \\ -K(-\varepsilon_0) & K(\varepsilon_0) \end{pmatrix} \begin{pmatrix} p_0(t) \\ p_1(t) \end{pmatrix}, \quad (4)$$

where, $p_{0/1}(t) \equiv (1 \mp \langle \sigma_z(t) \rangle)/2$ denotes the population at the lower (upper) level. The transition rates stand for the co-

operative process between the system and two reservoirs:

$$K(\pm\varepsilon_0) \equiv \frac{(\Delta/2)^2}{2\pi} \int_{-\infty}^{\infty} C^\pm(\omega) d\omega, \quad (5)$$

$$C^\pm(\omega) \equiv C_L(\pm\varepsilon_0 \mp \omega) C_R(\pm\omega),$$

with $C_\nu(\omega) \equiv \int_{-\infty}^{\infty} e^{i\omega t - Q_\nu(t)} dt$ denoting the probability density of the bath ν to absorb the energy ω (equivalently, to release the energy $-\omega$). Employing the Gaussian statistics of the “momentum” operator $\Omega(t)$, we have $Q_\nu(t) \equiv \langle [\Omega(0) - \Omega(t)] \Omega(0) \rangle = \int_0^\infty \frac{J_\nu(\omega)}{\pi\omega^2} [\coth(\frac{\omega}{2T_\nu}) (1 - \cos(\omega t)) + i \sin(\omega t)] d\omega$ [22], with $J_\nu(\omega) = 4\pi \sum_j \lambda_{j,\nu}^2 \delta(\omega - \omega_{j,\nu})$ being the spectral density of the bosonic bath ν . In contrast to the Redfield-weak coupling scheme [10, 12], the rate expressions (5) distinctly exhibit the non-resonant energy tunneling processes, conjoining the two baths nonadditively: $K(\varepsilon_0)$ means when the central system loses energy ε_0 by relaxing from the upper level to the lower one, the R bath will absorb ω and the L bath gains the rest if $\varepsilon_0 > \omega$ or even supplements the shortage if $\omega > \varepsilon_0$; $K(-\varepsilon_0)$ depicts the similar energy transfer process for the central system exciting from the lower level to the upper one.

Generating function and geometric heat flux. Following the *Full Counting Statistics* [24, 25], we next construct the cumulant generating function (CGF) of the NESB model to count the phonon energy transfer through the right system-bath coupling [10, 11, 18, 26–28]. Denote $\rho_t(n, \omega)$ as the joint probability that a total energy of ω has been transferred to the right bath during time interval $[0, t]$, with the two-level system populates at state $|n\rangle$ ($n = 0, 1$) at time t , we then introduce the characteristic function of that joint probability $|z(\chi, t)\rangle \equiv (\int_{-\infty}^{\infty} \rho_t(0, \omega) e^{i\omega\chi} d\omega, \int_{-\infty}^{\infty} \rho_t(1, \omega) e^{i\omega\chi} d\omega)^T$ with the energy counting field χ . Following [17], this characteristic function satisfies the following dynamics:

$$\frac{d}{dt} |z(\chi, t)\rangle = -\hat{\mathcal{H}}(\chi) |z(\chi, t)\rangle, \quad (6)$$

$$\text{with } \hat{\mathcal{H}}(\chi) = \begin{pmatrix} K(-\varepsilon_0) & -K^+(\chi) \\ -K^-(\chi) & K(\varepsilon_0) \end{pmatrix},$$

where $K^\pm(\chi) \equiv \frac{(\Delta/2)^2}{2\pi} \int_{-\infty}^{\infty} C^\pm(\omega) e^{\pm i\omega\chi} d\omega$. When the counting field $\chi = 0$, $K^\pm(0) = K(\pm\varepsilon_0)$ and in turn Eq. (6) reduces to Eq. (4). Thus, the characteristic function of the heat transfer is $Z(\chi, t) = \int_{-\infty}^{\infty} (\rho_t(0, \omega) + \rho_t(1, \omega)) e^{i\omega\chi} d\omega$ and the CGF is $\mathcal{G}(\chi) \equiv \lim_{t \rightarrow \infty} \frac{1}{t} \ln[Z(\chi, t)]$, which generates the n -order cumulant of heat transfer fluctuations through $\lim_{t \rightarrow \infty} \langle \langle Q^n \rangle \rangle / t = \partial_{i\chi}^n \mathcal{G}(\chi)|_{\chi=0}$. The mean value of the heat flux is just the first order: $J = \partial_{i\chi} \mathcal{G}(\chi)|_{\chi=0}$.

Behaviors in the long time limit are of our central interest. They are governed by the ground state of the operator $\hat{\mathcal{H}}(\chi)$, of which the eigenvalue $E_0(\chi)$ possesses the the smallest real part. For time-independent $\hat{\mathcal{H}}(\chi)$, $\lim_{t \rightarrow \infty} Z(\chi, t) \sim e^{-E_0(\chi)t}$ and in turn $\lim_{t \rightarrow \infty} \langle \langle Q^n \rangle \rangle / t = -\partial_{i\chi}^n E_0(\chi)|_{\chi=0}$. However, for time-dependent $\hat{\mathcal{H}}(\chi, t)$, where the system parameters $\Delta(t)$, $\varepsilon_0(t)$, the bath temperature $T_\nu(t)$ or the system-bath coupling $\lambda_{j,\nu}(t)$ could be subject to periodic modulations, the adiabatic geometric phase effect has been

unravelling to play an important role in the dynamic control of energy transfer [10, 11]. In this case, although at every instant the dynamics (6) is preserved, there exist two contributions in the CGF: $\lim_{t \rightarrow \infty} Z(\chi, t) \sim e^{t\mathcal{G}} = e^{t(\mathcal{G}_{dyn} + \mathcal{G}_{geom})}$. One is the dynamic part \mathcal{G}_{dyn} , and the other is the geometric part \mathcal{G}_{geom} [10, 11, 28]:

$$\begin{aligned}\mathcal{G}_{dyn} &= -\frac{1}{\mathcal{T}_p} \int_0^{\mathcal{T}_p} dt E_0(\chi, t), \\ \mathcal{G}_{geom} &= -\frac{1}{\mathcal{T}_p} \int_0^{\mathcal{T}_p} dt \langle \phi_0 | \partial_t | \psi_0 \rangle,\end{aligned}\quad (7)$$

with \mathcal{T}_p the modulating period [29] and $|\psi_0\rangle(\langle\phi_0|)$ the bi-orthonormal right (left) eigenvector corresponding to the ground state of $\hat{H}(\chi, t)$ [30]. In the case of two parameters being modulated, say $u_1(t), u_2(t)$, the calculation of \mathcal{G}_{geom} can be done using Stokes theorem [31],

$$\mathcal{G}_{geom} = -\frac{1}{\mathcal{T}_p} \iint_{u_1 u_2} du_1 du_2 \mathcal{B}_{u_1 u_2} \quad (8)$$

and the Berry curvature [31, 32] is:

$$\begin{aligned}\mathcal{B}_{u_1 u_2} &= \langle \partial_{u_1} \phi_0 | \partial_{u_2} \psi_0 \rangle - \langle \partial_{u_2} \phi_0 | \partial_{u_1} \psi_0 \rangle \\ &= \frac{\langle \phi_0 | \partial_{u_1} \hat{H} | \psi_1 \rangle \langle \phi_1 | \partial_{u_2} \hat{H} | \psi_0 \rangle - (u_1 \leftrightarrow u_2)}{(E_0 - E_1)^2}.\end{aligned}\quad (9)$$

with E_1 the eigenvalue of the excited state and $|\psi_1\rangle(\langle\phi_1|)$ the corresponding bi-orthonormal right (left) eigenvector. According to these formulas, we have the dynamic heat flux J_{dyn} and the geometric heat flux J_{geom} ,

$$J_{dyn} = -\frac{1}{\mathcal{T}_p} \int_0^{\mathcal{T}_p} dt \left. \frac{\partial E_0(\chi, t)}{\partial(i\chi)} \right|_{\chi=0}, \quad (10)$$

$$J_{geom} = -\frac{1}{\mathcal{T}_p} \iint_{u_1 u_2} du_1 du_2 \left. \frac{\partial \mathcal{B}_{u_1 u_2}}{\partial(i\chi)} \right|_{\chi=0}. \quad (11)$$

Results and discussions. With equations above, we are ready to study the consequences of dynamic control of the NESB model in a more exact way, *i.e.*, without Redfield-weak coupling approximation.

i) Unbiased case, $\varepsilon_0 = 0$. In this degenerate case, we have $K(-\varepsilon_0) = K(\varepsilon_0)$, $K^+(\chi) = K^-(\chi)$, and the matrix,

$$\hat{H}(\chi, t) = \begin{pmatrix} K(\varepsilon_0) & -K^+(\chi) \\ -K^+(\chi) & K(\varepsilon_0) \end{pmatrix}. \quad (12)$$

Thus, the corresponding eigenvalues and eigenvectors turn into a simple form,

$$\begin{aligned}E_{0/1} &= K(\varepsilon_0) \mp \tilde{K}^+(\chi), \\ |\psi_{0/1}\rangle &= \frac{1}{\sqrt{2}} \begin{pmatrix} \pm 1 & 1 \end{pmatrix}^T, \quad \langle \phi_{0/1} | = \frac{1}{\sqrt{2}} \begin{pmatrix} \pm 1 & 1 \end{pmatrix}.\end{aligned}$$

Since the eigenvectors are constant, we have that for whatever two-parameter modulations, the Berry curvature $\mathcal{B}_{u_1 u_2} \equiv 0$. There is no geometric phase effect and geometric heat flux is

absent when the two-level energy gap is zero. This result is independent of the system-bath coupling strength.

Note that, in contrast to the absence of geometric heat flux here, Ref. [10] treats the same physical system with $\varepsilon_0 = 0$, but in the Redfield-weak coupling scheme and in the basis of Hamiltonian (2) (with notation $\Delta \rightarrow \omega_0$). Nonzero geometric heat flux is investigated there. The difference probably comes from two folds: 1) the effect of the non-resonant tunneling and collective nonadditive interacting between the system and baths in NIBA scheme, are inherently overlooked in the Redfield-weak coupling approximation; 2) the rotation difference of the basis. Generally, the different choice of basis should not lead to different physical results. But in order to get the final population dynamics, the secular approximation are applied for both methods, to decouple the diagonal and non-diagonal reduced density matrix elements [33]. In this sense, after neglecting the off-diagonal dynamics, the two populations in the upper/lower level in the rotated Hamiltonian (2) [$p_{0/1}(t) \equiv (1 \mp \langle \sigma_x(t) \rangle)/2$] are different from the populations in the Hamiltonian (1) [$p_{0/1}(t) \equiv (1 \mp \langle \sigma_z(t) \rangle)/2$]. To a final conclusion of the difference, a detailed study of the full reduced density matrix dynamics is in demand.

Any way, although it has been known already that the dynamic heat flux for the same Hamiltonian calculated from the two methods are different for *intermediate* coupling strength and essentially the same in the weak coupling limit [17], here we for the first time show the difference for *whatever* coupling strength with geometric heat flux. Since the geometric phase effect contains the high-order heat transfer fluctuations, we expect that the geometric heat flux could be an effective tool to compare the difference or even judge the correctness of various approximation schemes.

ii) Biased case, $\varepsilon_0 \neq 0$. An applied magnetic field could control this Zeeman splitting. In this nondegenerate case, there do exist the geometric heat flux. In the following, to simplify the calculation we assume Marcus limit [22, 34] that works in high temperature $T_\nu > \varepsilon_0$ and/or strong system-bath coupling regime. The Marcus limit could be approached by a short time expansion of $Q_\nu(t)$ such that $Q_\nu(t) = \Gamma_\nu T_\nu t^2 + i\Gamma_\nu t$ with the renormalized system-bath coupling $\Gamma_\nu = \int \frac{J_\nu(\omega)}{\pi\omega} d\omega = \sum_j 4\lambda_{j,\nu}^2 / \omega_{j,\nu}$. In this way, we have the transition rates [17, 22]:

$$\begin{aligned}C_\nu(\omega) &= \frac{\Delta}{2} \sqrt{\frac{\pi}{\Gamma_\nu T_\nu}} \exp \left[-\frac{(\omega - \Gamma_\nu)^2}{4\Gamma_\nu T_\nu} \right], \\ K(\pm\varepsilon_0) &= \frac{\Delta^2}{4} \sqrt{\frac{\pi}{\Gamma_L T_L + \Gamma_R T_R}} \exp \left[-\frac{(\varepsilon_0 \mp \Gamma_L \mp \Gamma_R)^2}{4(\Gamma_L T_L + \Gamma_R T_R)} \right],\end{aligned}$$

where $\Delta, \varepsilon_0, T_\nu, \Gamma_\nu$ could be subject to the dynamic control. By substituting these rates into the dynamics. (6), we are able to investigate the Berry curvature and the geometric heat flux J_{geom} through Eqs. (9) and (11).

We first adiabatically modulate the two bath temperatures. The external control frequency Ω_p is chosen to be sufficiently small so that the adiabatic condition is respected [29]. The protocol is chosen as $T_L(t) = 150 + 90 \cos(\Omega_p t)$ (K), $T_R(t) = 150 + 90 \sin(\Omega_p t)$ (K), so that there is no temperature-bias-induced flux on average ($J_{dyn} = 0$), but the geometric heat

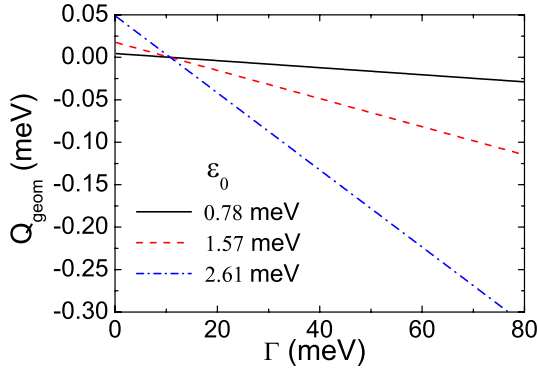


FIG. 2: (color online). Integrated geometric heat flux per period $Q_{geom} \equiv J_{geom} \mathcal{T}_p$ as a linear function of the system-bath coupling under the two-bath-temperature modulation. We set the symmetric coupling $\Gamma_L = \Gamma_R = \Gamma$ and tunnelling energy is $\Delta = 5.22$ meV. When $\varepsilon_0 \rightarrow -\varepsilon_0$, we observe the same lines.

flux emerges. Figure 2 shows that the integrated geometric heat flux per period $Q_{geom} \equiv J_{geom} \mathcal{T}_p$ is linearly dependent on the system-bath coupling Γ . When Γ approaches to zero, Q_{geom} does not vanish but persists at some finite values. Also, we find that increasing the gap ε_0 can increase Q_{geom} and when $\varepsilon_0 \rightarrow -\varepsilon_0$, we observe the same lines. Generally, reversing the modulation cycle can reverse the direction of geometric heat flux. Moreover, as indicated in Fig. 2, when the coupling strength Γ exceeds some threshold values the geometric heat flux will also reverse its direction. This may offer a useful mean in dynamic control of the heat flux induced by adiabatic periodic modulation.

Second, we manipulate the bath temperature and the two-level energy gap ε_0 . As shown in Fig. 3(a), Q_{geom} is linearly dependent on the system-coupling strength. When Γ approaches to zero, Q_{geom} vanishes. Raising the average level-gap $\bar{\varepsilon}_0$ is able to increase the magnitude of Q_{geom} . If we reverse $\bar{\varepsilon}_0 \rightarrow -\bar{\varepsilon}_0$, the geometric heat flux reverses its direction so that when $\bar{\varepsilon}_0 = 0$, Q_{geom} is absent. Although in this modulation protocol the dynamic heat flux is nonzero, it decays

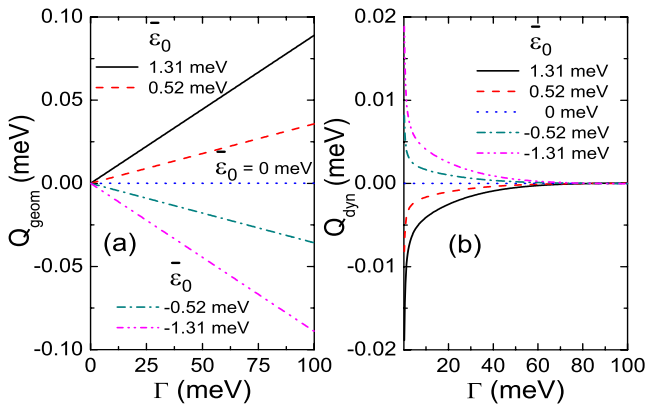


FIG. 3: (color online). (a) Q_{geom} as a linear function of Γ under modulations of one bath temperature and the gap $\varepsilon_0(t)$. We set $T_L(t) = 150 + 90 \cos(\Omega_p t)$ (K), $\varepsilon_0(t) = \bar{\varepsilon}_0 + 0.78 \sin(\Omega_p t)$ (meV). $T_R = 150$ K, $\Delta = 5.22$ meV. (b) Integrated dynamic heat flux per period $Q_{dyn} \equiv J_{dyn} \mathcal{T}_p$ under the same conditions for comparison.

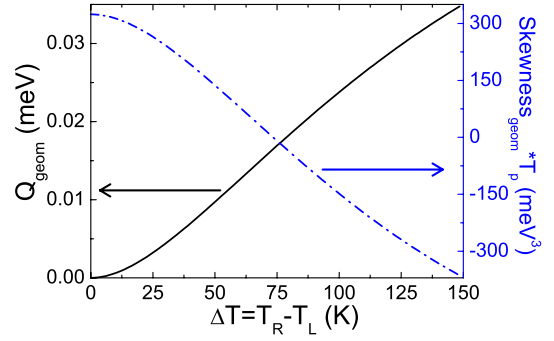


FIG. 4: (color online). Emergence of geometric phase effect and geometric heat flux for modulating two system-bath couplings. Although Q_{geom} is absent at $T_L = T_R$, the nonzero geometric skewness ($\partial_{i\chi}^3 \mathcal{G}_{geom}|_{\chi=0}$) shows the existence of the geometric phase effect, manifesting itself as the high-order heat transfer fluctuations. The control protocol is $\Gamma_L = 130.5 + 104.4 \cos(\Omega_p t)$ (meV) and $\Gamma_R = 130.5 + 104.4 \sin(\Omega_p t)$ (meV). Other parameters are $T_L = 150$ K, $\omega_0 = 2.61$ meV and $\Delta = 5.22$ meV.

very fast as the system-bath coupling Γ increases, [see Fig. 3(b)]. In this way, the geometric heat flux will dominate the energy transport in the strong system-bath coupling regime.

Besides these two control protocols discussed above, we finally consider the special case of modulating two system-bath couplings $\Gamma_L(t)$ and $\Gamma_R(t)$. Figure 4 shows the emergence of geometric heat flux when $T_L \neq T_R$. Although at $T_L = T_R$, the geometric heat flux vanishes, the geometric phase effect still exists, manifesting itself as the high-order heat transfer fluctuation, *e.g.*, the nonzero geometric skewness $\partial_{i\chi}^3 \mathcal{G}_{geom}|_{\chi=0} \neq 0$. These observations are distinct from the previous results either in quantum weak-coupling regime [10] or classical regime [11], wherein under couplings-modulation, the Berry curvatures are always zero (no matter what other parameter settings), so that the geometric phase effect and geometric heat flux are always absent. It is the strong system-bath coupling we consider here that makes the couplings-modulation-induced geometric heat pump nontrivial.

In summary, we have studied the geometric phase induced heat flux extensively in the spin-boson system under the adiabatic periodical modulation without the Redfield approximation. Using NIBA approach, we have found that there exists the geometric heat flux only when the two level system's energy gap is not zero. This result shows that NIBA and the Redfield approximation can give different results for the same physical system even when the coupling is weak. Moreover, the pumping, no pumping, and dynamic control of geometric heat flux have been discussed in detail. In particular, two system-bath couplings modulation induced geometric heat flux has been identified. So far, this nontrivial observation is exclusively for quantum transport in the strong system-bath coupling regime.

We thank Baowen Li for useful discussions. This work was supported in part by the 10000-Plan of Shandong province, and the National High-Tech Program of China grant No. 2011AA010800 and 2011AA010803, NSFC grant No. 11174177 and 60725416. J.R. acknowledges the support of the U.S. Department of Energy through the LANL/LDRD

Program.

-
- [1] N. Li, J. Ren, L. Wang, G. Zhang, P. Hänggi, and B. Li, Rev. Mod. Phys. **84**, 1045 (2012).
 - [2] D. Segal and A. Nitzan, Phys. Rev. E **73**, 026109 (2006).
 - [3] R. Marathe, A. M. Jayannavar, and A. Dhar, Phys. Rev. E **75**, 030103(R) (2007).
 - [4] N. Li, P. Hänggi, and B. Li, Europhys. Lett. **84**, 40009 (2008); J. Ren and B. Li, Phys. Rev. E **81**, 021111 (2010).
 - [5] W. Zhang and B. Hu, Phys. Rev. B **81**, 205401 (2010).
 - [6] S. Zhang, J. Ren, and B. Li, Phys. Rev. E **84**, 031122 (2011); B. Ai, D. He, and B. Hu, Phys. Rev. E **81**, 031124 (2010).
 - [7] A. Dhar, O. Narayan, A. Kundu, and K. Saito, Phys. Rev. E **83**, 011101 (2011).
 - [8] K. Kovhannisyanyan and A. E. Allahverdyan, J. Stat. Mech. **P06010** (2010).
 - [9] S. Narayana and Y. Sato, Phys. Rev. Lett. **108**, 214303 (2012).
 - [10] J. Ren, P. Hänggi, and B. Li, Phys. Rev. Lett. **104**, 170601 (2010).
 - [11] J. Ren, S. Liu, and B. Li, Phys. Rev. Lett. **108**, 210603 (2012).
 - [12] D. Segal and A. Nitzan, Phys. Rev. Lett. **94**, 034301 (2005).
 - [13] L. A. Wu, C. X. Yu, and D. Segal, Phys. Rev. E **80**, 041103 (2009); L. A. Wu and D. Segal, *ibid.*, **83**, 051114 (2011).
 - [14] T. Ruokola and T. Ojanen, Phys. Rev. B **83**, 045417 (2011).
 - [15] K. A. Velizhanin, H. Wang, and M. Thoss, Chem. Phys. Lett. **460**, 325 (2008).
 - [16] L. Nicolin and D. Segal, Phys. Rev. B **84**, 161414(R) (2011).
 - [17] L. Nicolin and D. Segal, J. Chem. Phys. **135**, 164106 (2011).
 - [18] C. Wang, J. Ren, B. Li, and Q. H. Chen Eur. Phys. J. B **85**, 110 (2012).
 - [19] F. Nesi, E. Paladino, M. Thorwart, and M. Grifoni, Phys. Rev. B **76**, 155323 (2007).
 - [20] A. J. Legget, S. Chakravarty, A. T. Dorsey, M. P. A. Fisher, A. Garg, and W. Zwerger, Rev. Mod. Phys. **59**, 1 (1987).
 - [21] H. Dekker, Phys. Rev. A **35**, 1436 (1987).
 - [22] U. Weiss, *Quantum Dissipative Systems* (Singapore, 2008).
 - [23] G. D. Mahan, *Many-Particle Physics* (New York, 2000).
 - [24] M. Esposito, U. Harbola, and S. Mukamel, Rev. Mod. Phys. **81**, 1665 (2009).
 - [25] M. Campisi, P. Hänggi, and P. Talkner, Rev. Mod. Phys. **83**, 771 (2011).
 - [26] D. A. Bagrets and Y. V. Nazarov, Phys. Rev. B **67**, 085316 (2003).
 - [27] I. V. Gopich and A. Szabo, J. Chem. Phys. **124**, 154712 (2006).
 - [28] N. A. Sinitsyn and I. Nemenman, Europhys. Lett. **77**, 58001 (2007); N. A. Sinitsyn, J. Phys. A: Math. Theor. **42**, 193001 (2009).
 - [29] To satisfy the adiabatic condition, $\mathcal{T}_p = 2\pi/\Omega_p$ should be much larger than the characteristic relaxation time of the whole system, including the dynamics of the two-level system and the baths. Also, \mathcal{T}_p should be much larger than the relaxation time of the two population dynamics: $\mathcal{T}_c = 1/(E_1 - E_0)|_{\chi=0}$ [11]. In our choosing parameters, the systems relaxation time \mathcal{T}_c is on the order of ps. Thus, the adiabatic condition can be satisfied when the modulation frequency $\Omega_p \ll 1$ THz. We choose $\Omega_p = 1$ ns throughout the calculations.
 - [30] Different from the conventional Dirac's representation, the bracket notation we choose here just denotes the left-right eigenvector relation. They are not the conjugate transpose of each other.
 - [31] D. Xiao, M.-C. Chang, and Q. Niu, Rev. Mod. Phys. **82**, 1959 (2010).
 - [32] M. V. Berry, Proc. R. Soc. Lond. A **392**, 45 (1984).
 - [33] H.-P. Breuer and F. Petruccione, *The Theory of Open Quantum Systems* (New York, 2002).
 - [34] R. A. Marcus, J. Chem. Phys. **24**, 966 (1956).